Model of crop growth, water flow, and solute transport in layered soil

Shuai Chen [a], Xiaomin Mao[a,*], David Andrew Barry [b], Jian Yang [a]

[a] College of Water Resources and Civil Engineering, China Agricultural University, Beijing, 100083, PR China. Emails: slsdchen@163.com, maoxiaomin@cau.edu.cn, cauyangjian@126.com

[b] Ecological Engineering Laboratory (ECOL), Environmental Engineering Institute (IIE), Faculty of Architecture, Civil and Environmental Engineering (ENAC), Ecole polytechnique fédérale de Lausanne (EPFL), 1015 Lausanne, Switzerland. Email: andrew.barry@epfl.ch

∗ Corresponding author: Dr. Xiaomin Mao
Centre for Agricultural Water Research in China
China Agricultural University
Tsinghuadong Street No.17, Beijing 100083, P.R. China
Tel: (8610) 6273-8498
Fax: (8610) 6273-6533
E-mail: maoxiaomin@cau.edu.cn

Abstract

Agro-eco-hydrological models are essential for managing scarce water resources and ensuring crop productivity. Here, a one-dimensional agro-eco-hydrological model, LAWSTAC, capable of simulating water and solute transport in layered soil coupled with crop growth, is presented and validated. LAWSTAC considers eight hydraulic conductivity discretization methods to address the nonlinearity of Richards equation for soil water flow. LAWSTAC includes two root water uptake models and a flexible root distribution model for reliable transpiration simulation. Layered soil infiltration simulated by the eight discretization methods showed the arithmetic mean, geometric mean or the triadic mean got better results. The model was further verified by comparison with results from two widely used models, HYDRUS-1D and SWAP, using field-measured wheat growth data for 2007 and 2008 in the Northwest China. The models produced similar results for flow in layered soil, although SWAP showed some instability in the salinity dynamics. LAWSTAC models crop growth with a more efficient parameterization than SWAP. The root mean square errors of soil moisture , soil salinity concentration and *LAI* simulated by LAWSTAC were less than 0.06 cm^3 cm^{-3}, 3.56 g L^{-1}, and 0.43, respectively. In conclusion, LAWSTAC is suitable for simulating soil water and salinity dynamics, crop growth and their interactions.

Keywords: Hydrologic model; Crop growth model; Coupling; Layered soil

Software availability

Name of software: LAWSTAC

Developers: Shuai Chen and Xiaomin Mao

Contact: slsdchen@163.com, maoxiaomin@cau.edu.cn

Year first available: 2016

Hardware required: Personal computer

Software required: Microsoft Windows operating system

Program languages: MATLAB

Availability and cost: Contact the authors, free for non-commercial use.

1. Introduction

Water shortages and soil salinization are two major factors that negatively affect agricultural productivity (Molden, 1997; Cominelli et al., 2013). To avoid such negative impacts, quantification of crop growth as well as water and solute transport are necessary for development of appropriate policies and measures. Often, field experiments are conducted to investigate the appropriateness of agricultural management practices that aim to enhance water use efficiency and grain production under limited water supply and soil salinization situations (Tuong and Bhuiyan, 1999; Kahlown and Azam, 2003). However, field experiments with different crops under various soil, water, salinity, and environment conditions are expensive, laborious and time consuming, especially for long term experiments that involve frequent measurements. Process-based simulation tools enhance the insights gained from long term experiments and potentially improve understanding of crop growth and yield under different hydrological and environmental conditions. Validated models also permit prognostic exploration of different strategies to improve crop yield and to maintain soil resilience.

Many one-dimensional (1D) physically based models simulating water and solute dynamics in variably saturated-unsaturated soil in field scale are available, e.g., LEACHM (Leaching Estimating and Chemistry model; Hutson and Wagenet, 1995), SWAP (Soil Water Atmosphere Plant; van Dam et al., 1997), RZWQM (Root Zone Water Quality Model; Hanson et al., 1998) and HYDRUS-1D (Simunek et al., 2005). Recent studies used these models to quantify soil water and solute transport processes under different boundary conditions with or without plant interactions (Cameira et al., 2000; Kumar et al., 2015; Salamati et al., 2016). As indicated above, agricultural systems models can be used as planning tools to determine agricultural management strategies under different environmental scenarios. Widely used agricultural systems models include EPIC (Environmental Policy-Integrated Climate; Williams et al., 1989), APSIM (Agricultural Production Systems Simulator; McCown et al., 1996),

WOFOST (World Food Studies; Boogaard et al., 1998) and DSSAT (Decision Support System for Agrotechnology Transfer; Jones et al., 2003). In the agricultural systems models, the simulation of evapotranspiration, soil water content and salt content level is one of the key points for calculation (Eitzinger et al., 2004). The water loss through evaporation and transpiration can determine the water distribution in the soil profiles, thus affecting the dynamics of salt content. Meanwhile, the variation in soil moisture and salt content are two main causes of crop yield variation in a soil-plant system. Crops consume soil water in the root zone through root uptake. The interaction between crop growth and soil conditions is complex, although it is an important physical and physiological process in agro-ecological system. Consequently, coupling of hydrologic and agricultural systems models can connect the hydrology and agricultural and better understand agro-eco-hydrological process in agricultural regions.

Ma et al. (2006) coupled the CERES-Maize agricultural systems model with RZWQM to address soil and water quality issues with a more comprehensive plant growth description. A recent integrated simulation model for improving water use efficiency and crop yields was reported by Zhou et al. (2012), who linked WOFOST with HYDRUS-1D to optimize irrigation scheduling for spring wheat in Northwest China. Later, Kumar et al. (2015) used SWAP (with WOFOST embedded) to simulate soil moisture and solute dynamics along with wheat yields under various saline water irrigation regimes in New Delhi, India. Despite these efforts, issues remain to be addressed for more accurate simulation in the agro-eco-hydrological system. For example, HYDRUS-1D assumes a fixed root distribution pattern when root growth is considered, which might not account for the actual root water uptake. In addition, an aboveground crop growth model is absent in HYDRUS. The algorithm for solving the solute transport equation in SWAP adopts an explicit temporal discretization, which is prone to instability under abrupt variations of soil water content (Xu et al., 2016). The coupled CERES/RZWQM model (Ma et al., 2006) combines the advantages of both a comprehensive description of specific crop growth and reliable predictions of water

and nutrient distribution in the root zone. However, its performance for distinctly layered soils, which are common in the field, is unclear because it is limited to a fixed number of soil layers (Sophocleous et al., 2009). Furthermore, no specific attention is paid to the model's performance under such a condition.

Although Wang et al. (2014) showed that their Richards equation-based models were capable of simulating water flow in layered soils, simulations usually encountered difficulties in achieving water balance and produced numerical oscillations (Lima-Vivancos and Voller, 2004). Due to the nonlinearity of hydraulic conductivity in unsaturated soils, numerical models must incorporate strategies to reliably simulate water movement. Typically, agro-eco-hydrological models adopt a fixed averaging method to calculate the internodal conductivities (Simunek et al., 2005). Alternative methods could improve accuracy and stability of simulation results under different soil structure conditions. Recent progress in techniques of remote sensing and GIS, etc. have advanced the quantification of regional eco-hydrologic systems. The spatial and temporal scales involved require coupling between regional groundwater flow models and flow models in the unsaturated zone, especially in agricultural areas where layered soil profiles are common (Li et al., 2017) and solute transport simulations are required. For practical applications, models for such areas should be process-based, computationally efficient, and with robust parameterizations.

The objectives of this study are (a) to develop an efficient model, LAWSTAC, for simulating crop growth and the associated water and solute dynamics in layered soils, (b) to evaluate various conductivity-averaging methods used in LAWSTAC for layered soil, and (c) to assess the capabilities and performance of the model by comparing its results with the widely used HYDRUS-1D and SWAP models, based on a spring wheat growth experiment in Northwest China.

2. Description of LAWSTAC

LAWSTAC is a process-based model that simulates vertical 1D saturated-unsaturated water flow and solute transport in layered soils, together with crop growth. The soil water and solute transport processes are described through the Richards equation (RE) and advection-dispersion equation (ADE), respectively. The crop growth processes are driven by air temperature and solar radiation. Eight different averaging methods are considered in the model for computing the hydraulic conductivity in the middle of two adjacent nodes. The model is compiled in the MATLAB programming language, which can be easily transformed to a standalone executable, for instance to be called by a regional-scale hydrologic model.

2.1 Soil water flow

Soil water flow in the soil profile is described by the RE,

$$\frac{\partial \theta}{\partial t} = \frac{\partial}{\partial z}\left[K(h)\left(\frac{\partial h}{\partial z} - 1\right)\right] - S \tag{1}$$

where t is time (d), z is the vertical space coordinate in the downward direction from the soil surface (cm), θ is the soil volumetric water content ($cm^3\ cm^{-3}$), h is soil matric potential in the unsaturated zone or water pressure head in the saturated zone (cm), K is the hydraulic conductivity ($cm\ d^{-1}$), S is a sink term, defined as soil water extraction rate by plant roots ($cm^3\ cm^{-3}\ d^{-1}$). This "mixed" form RE is generally preferred to the θ-based or h-based forms due to its superior performance in mass conservation while avoiding potential disadvantages, e.g., discontinuity of θ at the interface of two soil layers of the θ-based form (Celia et al., 1990).

When we solve the "mixed" form RE, descriptions of relationships among θ, h and K are required. The Brooks-Corey-Burdine and van Genuchten-Mualem (VGM) models are both widely used for this purpose (An and Noh, 2014). In this model, the soil water retention and hydraulic conductivity are expressed through the VGM model (Mualem, 1976; van Genuchten, 1980),

$$\theta(h)=\begin{cases}\theta_r+\dfrac{\theta_s-\theta_r}{\left(1+|\alpha h|^n\right)^{1-1/n}} & h<0\\ \theta_s & h\geq 0\end{cases} \tag{2}$$

$$S_e=\frac{\theta-\theta_r}{\theta_s-\theta_r} \tag{3}$$

$$K=K_sS_e^l\left[1-\left(1-S_e^{n/(n-1)}\right)^{1-1/n}\right]^2 \tag{4}$$

where θ_s is the saturated water content (cm^3 cm^{-3}), θ_r is the residual water content (cm^3 cm^{-3}), K_s is the saturated hydraulic conductivity (cm d^{-1}), α is an air-entry parameter (cm^{-1}), n is a pore size distribution parameter, and l is a pore connectivity parameter.

We specify the water content or soil matric potential within the flow domain at the initial time (t=0) as the initial condition,

$$\theta(z,t)=\theta_0(z),\quad 0\leq z\leq L, t=0 \tag{5}$$

$$h(z,t)=h_0(z),\quad 0\leq z\leq L, t=0 \tag{6}$$

where $\theta_0(z)$ is initial water content at different soil depths (cm^3 cm^{-3}), $h_0(z)$ is initial soil matric potential or water pressure head at different soil depths (cm), and L is the maximum soil depth under consideration (cm). The boundary conditions at the soil surface (z = 0) or at the base (z = L) of the soil profile are expressed as specified pressure head, specified flux or specified gradient boundary conditions (Simunek et al., 1999),

$$h(z,t)=h_0(t),\qquad z=0 \text{ or } L,\ t>0 \tag{7}$$

$$K\left(1-\frac{\partial h}{\partial z}\right)=q_0(t),\ z=0 \text{ or } L,\ t>0 \tag{8}$$

$$\frac{\partial h}{\partial z}=0,\qquad z=L,\ t>0 \tag{9}$$

where $h_0(t)$ (cm) and $q_0(t)$ (cm d^{-1}) are pressure head and soil water flux (due to irrigation, precipitation, evaporation, drainage, etc.) at the upper or lower boundary, respectively.

2.2 Solute transport

Solute transport is described by the ADE. For conservative species, neglecting adsorption, degradation, etc., the 1D governing equation is,

$$\frac{\partial(\theta \cdot c)}{\partial t} = \frac{\partial}{\partial z}\left[D_{sh}(v,\theta)\frac{\partial c}{\partial z}\right] - \frac{\partial(q \cdot c)}{\partial z} - S_s \tag{10}$$

where c is solute concentration in soil water (g cm^{-3}), q is soil water flux (cm d^{-1}), S_s is the solute sink term accounting for uptake by root (g cm^{-3} d^{-1}), and D_{sh} is the effective dispersion coefficient (cm^2 d^{-1}), D_{sh} is given by (Bear, 1972),

$$D_{sh}(v,\theta) = D_L q + \theta D_0 \tau_w \tag{11}$$

where D_L is the longitudinal dispersivity (cm), D_0 is the molecular diffusion coefficient in free water (cm^2 d^{-1}), that is related to the solute and temperature, and τ_w is a tortuosity factor in the liquid phase, that is a function of the water content (Millington and Quirk, 1961),

$$\tau_w = \theta^{7/3} / \theta_s^2 \tag{12}$$

The solute sink term S_s can be written as,

$$S_s = K_r c S \tag{13}$$

where K_r is a parameter accounting for relative uptake of solutes by roots.

The initial condition is,

$$c(z,t) = c_0(z), \qquad 0 \le z \le L,\ t = 0 \tag{14}$$

where $c_0(z)$ is initial solute concentration in the soil profile (g cm^{-3}). The boundary conditions at the soil surface ($z = 0$) or at the bottom ($z = L$) of the soil profile can be expressed as Dirichlet, Neumann or Cauchy types,

$$c(z,t) = c_0(t), \qquad z = 0 \text{ or } L,\ t > 0 \tag{15}$$

$$\frac{\partial c}{\partial z} = 0, \qquad z = 0 \text{ or } L,\ t > 0 \tag{16}$$

$$qc - D_{sh}\frac{\partial c}{\partial z} = q_0 c_I, \qquad z = 0 \text{ or } L,\ t > 0 \tag{17}$$

where $c_0(t)$ (g cm^{-3}) and q_0 (cm d^{-1}) are the solute concentration and fluid flux, respectively, at the surface or bottom boundaries, and c_I is the concentration of the

boundary fluid (g cm^{-3}).

2.3 Evaporation and transpiration

The reference evapotranspiration, ET_0, is calculated via the Penman-Monteith equation (Allen et al., 1998),

$$ET_0 = \frac{0.408\Delta(R_n - G) + \gamma \frac{900}{T+273} u_2 (e_s - e_a)}{\Delta + \gamma(1 + 0.34u_2)} \tag{18}$$

where R_n is net radiation at the crop surface (MJ m^{-2} d^{-1}), G is soil heat flux (MJ m^{-2} d^{-1}), T is air temperature at 2 m height above ground (°C), u_2 is wind speed at 2 m height (m s^{-1}), e_s is saturation vapor pressure (kPa), e_a is actual vapor pressure (kPa), Δ is slope of the saturation vapor pressure – temperature curve (kPa °C^{-1}), and γ is the psychrometric constant (kPa °C^{-1}).

The potential evapotranspiration ET_c is calculated using the crop coefficient, K_c, and ET_0,

$$ET_c = K_c ET_0 \tag{19}$$

Then, ET_c is partitioned into potential crop transpiration (T_p) and potential soil evaporation (E_p) based on the leaf area index (LAI) and extinction coefficient (β) (Childs and Hanks, 1975),

$$T_p = ET_c \left[1 - \exp(-\beta LAI)\right] \tag{20}$$

$$E_p = ET_c - T_p \tag{21}$$

Under soil water and/or salinity stresses, the actual soil evaporation and crop transpiration will be reduced. In this model, the actual evaporation from the soil surface is calculated based on a three-stage evaporation process,

$$\frac{E_a}{E_p} = \begin{cases} 0 & \theta_{sur} \le \theta_1 \\ \frac{\theta_{sur} - \theta_1}{\theta_2 - \theta_1}(1 + k_p h_s) & \theta_1 < \theta_{sur} < \theta_2 \\ 1 + k_p h_s & \theta_{sur} \ge \theta_2 \end{cases} \tag{22}$$

where E_a is the actual soil evaporation rate (cm d^{-1}), θ_{sur} is the soil water content at the soil surface (cm^3 cm^{-3}), θ_1 (cm^3 cm^{-3}) and θ_2 (cm^3 cm^{-3}) are threshold values below (θ_1) or above (θ_2) which the actual evaporation rate becomes 0 or the potential value, respectively. θ_1 is usually equal to wilting point moisture, θ_2 is about 50-70% of field capacity, h_s is the osmotic pressure head (cm), k_p is a slope coefficient (recommended 1.5×10^{-4}). The calculated E_a is taken as soil water flux at the upper boundary in the non-infiltration period and used in the specified flux boundary condition, Eq. (8). The actual transpiration is assumed to be equal to the root uptake, calculated either by the Feddes model (Feddes et al., 1974) or using an S-shaped function (van Genuchten, 1987), as described in detail in Section 2.4.

2.4 Root development and water uptake

The time-varying root development characteristics are described by the root length and the root density distribution along the soil profile. In the model, the root length can be given either according to periodically measured experimental data or by the root growth algorithm. For the root density distribution, we use a normalized spatial distribution function, $b(z)$, to quantify the spatial variation of water extraction by roots. The distribution function is expressed in two ways. The first function describes a linear relationship with soil depth (Shang et al., 2009),

$$b(z) = \frac{4m_r - 1}{Z_r(t)} - \frac{(8m_r - 4)z}{Z_r^2(t)} \tag{23}$$

where m_r is the ratio of root water uptake in the upper half of root zone to the total water uptake, commonly $1/2 \le m_r \le 3/4$. When $m_r = 1/2$, the function becomes (spatially) constant over root depth. The function $Z_r(t)$ is the maximum root depth at time t (cm). The second function is a piecewise linear relationship (Hoffman and van Genuchten, 1983),

$$b(z)=\begin{cases}\dfrac{5}{3Z_r(t)} & z\le\dfrac{1}{5}Z_r(t)\\ \dfrac{25}{12Z_r(t)}\left[1-\dfrac{z}{Z_r(t)}\right] & \dfrac{1}{5}Z_r(t)\le z\le Z_r(t)\\ 0 & z>Z_r(t)\end{cases} \tag{24}$$

We neglect variations in water storage inside plants. Assuming optimal environmental conditions, the integral of the potential root water uptake rate S_p (d^{-1}) with respect to z in the whole root zone is equal to the potential transpiration rate, T_p (cm d^{-1}),

$$\int_0^{Z_r(t)} S_p dz = T_p \tag{25}$$

When soil water is insufficient or soil salinity is high, the actual root water uptake, S, is decreased,

$$S=\alpha_w\alpha_s S_p=\alpha_w\alpha_s b(z)T_p \tag{26}$$

where α_w and α_s are water and salinity stress response functions of the root-water uptake, respectively. When the Feddes model (Feddes et al., 1974) is used,

$$\alpha_w=\begin{cases}0 & h>h_0, h<h_3\\ \dfrac{h-h_0}{h_1-h_0} & h_1<h\le h_0\\ 1 & h_2<h\le h_1\\ \dfrac{h-h_3}{h_2-h_3} & h_3<h\le h_2\end{cases} \tag{27}$$

$$\alpha_s=\begin{cases}1 & EC_{sat}\le EC_{\max}\\ 1-\left(EC_{sat}-EC_{\max}\right)\dfrac{EC_{slop}}{100}, & EC_{sat}>EC_{\max}\end{cases} \tag{28}$$

where h_0 is anaerobiosis point (cm), h_1 is pressure head below which roots uptake water at the maximum possible rate (cm), h_2 is pressure head below which roots can no longer uptake water at the maximum rate (cm), h_3 is the wilting point pressure head (cm), EC_{sat} is the electric conductivity of the soil saturation extract (dS m^{-1}), $EC_{\max}$ is the salinity threshold below which there is no salt stress on transpiration (dS m^{-1}), and EC_{slop} is the decline rate of root water uptake due to salinity stress (% m dS^{-1}). Since

root water uptake is affected by both soil conditions and atmospheric demand, h_2 is often defined as a function of T_p (Simunek et al., 2005),

$$h_2 = \begin{cases} h_2^L & T_p \le r_L \\ h_2^H + \dfrac{h_2^L - h_2^H}{r_H - r_L}\left(r_H - T_p\right) & r_L < T_p < r_H \\ h_2^H & T_p \ge r_H \end{cases} \tag{29}$$

where r_H (cm d^{-1}) and r_L (cm d^{-1}) are the potential transpiration rates below (r_L) or above (r_H) which h_2 becomes minimal (h_2^L) or maximal (h_2^H), respectively.

When the S-shaped function is used,

$$\alpha_w \alpha_s = \left[1 + \left(\frac{h + h_s}{h_{50}}\right)\right]^{-1} \tag{30}$$

where h_{50} represents the pressure head at which the water uptake rate is reduced by 50% during conditions of negligible osmotic stress (cm). The empirical constant p is approximately 3 for most crops.

2.5 Crop growth model

The model simulates crop growth based on daily temperature and solar radiation. The processes simulated include interception of solar radiation by the crop canopy, conversion of energy to biomass, and calculation of yield from biomass. Actual crop growth is constrained by water and temperature stress factors.

Phenological development of the crop is based on daily heat unit accumulation,

$$HU_k = \begin{cases} \dfrac{T_{min,k} + T_{max,k}}{2} - T_b, & HU_k \ge 0 \\ 0, & HU_k < 0 \end{cases} \tag{31}$$

where $T_{min,k}$ and $T_{max,k}$ are minimum temperature and maximum temperature for day k (°C) and T_b is the crop-specific base temperature (°C).

A heat unit index, *HUI*, governing leaf area growth and senescence, is calculated

as follows,

$$HUI_k = \frac{\sum_{w=1}^{k} HU_w}{PHU} \tag{32}$$

where *PHU* is the potential heat units required for crop maturity (°C).

The solar radiation intercepted by crop on day *k* is computed with Beer's law (Monsi and Saeki, 1953),

$$PARI_k = \frac{RA_k}{2}\left[1 - \exp\left(-\beta LAI_k\right)\right] \tag{33}$$

where *PARI* is the intercepted photosynthetic active radiation (MJ m^{-2}), and *RA* is solar radiation (MJ m^{-2}). The constant 1/2 is used to convert solar radiation to photosynthetic active radiation, and the value 13/20 is the extinction coefficient for crops with narrow row spacing (Uchijima et al., 1968).

The daily increase in biomass is estimated using,

$$\Delta B_{a,k} = (BE)(PARI_k)(REG_k) \tag{34}$$

where ΔB_a is daily actual increase in biomass (kg ha^{-1}), *BE* is the crop parameter for converting energy to biomass (kg ha^{-1} MJ^{-1} m^2), and *REG* is the crop growth regulating factor which is equal to the minimum value of Eqs. (35) and (36).

$$WS_k = \frac{T_{a,k}}{T_{p,k}} \tag{35}$$

$$TS_k = \sin\left[\frac{\pi}{2}\left(\frac{TG_k - T_b}{T_0 - T_b}\right)\right], \qquad 0 \le TS_k \le 1 \tag{36}$$

where *WS* and *TS* are the water and temperature stress factors, respectively, $T_{a,k}$ is actual transpiration on day *k* (cm d^{-1}), *TG* is the average daily temperature (°C), and T_0 is the crop optimal temperature (°C).

Calculation of daily *LAI* is divided into two different stages (Williams et al., 1989), the first being from emergence to the start of leaf senescence,

$$LAI_k = LAI_{k-1} + \Delta LAI \tag{37}$$

$$\Delta LAI = \Delta HUF \left\{1 - \exp\left[5\left(LAI_{k-1} - LAI_{\max}\right)\right]\right\} \sqrt{REG_k}\, LAI_{max} \tag{38}$$

where ΔLAI is the daily change in LAI, LAI_{max} is the maximum possible LAI, and HUF is the heat unit factor,

$$HUF_k = \frac{HUI_k}{HUI_k + \exp\left(ah_1 - ah_2 HUI_k\right)} \tag{39}$$

where ah_1 and ah_2 are crop parameters.

For the time from the start of leaf senescence to the end of growing season,

$$LAI_k = LAI_0 \left(\frac{1 - HUI_k}{1 - HUI_0}\right)^{L_r} \tag{40}$$

where L_r is a parameter that governs the LAI decline rate, LAI_0 is the maximum leaf area index under the crop stress, and HUI_0 is the value of HUI when LAI starts to decline.

Crop height is estimated using,

$$H_k = H_{max} \sqrt{HUF_k} \tag{41}$$

where H_k is crop height for day k (cm), and H_{max} is the maximum height (cm).

The daily change in root zone weight is computed by,

$$\Delta RW_k = \Delta B_{a,k}\left(ar_1 - ar_2 HUI_k\right) \tag{42}$$

where ΔRW_k is the change in root weight (kg ha^{-1}), and ar_1 and ar_2 are crop parameters with typical values of 0.4 and 0.2.

Root length is simulated as a function of heat unit index and potential root zone depth,

$$RD_k = \frac{5}{2} RD_{max} HUI_k \qquad RD \le RD_{\max} \tag{43}$$

$$RD_k = RD_{\max} \qquad RD > RD_{\max} \tag{44}$$

where RD is the root length (cm), RD_{max} is the maximum root length (cm), and the constant 5/2 allows root length to reach its maximum before physiological maturity.

The harvest index is used to estimate the crop yield. It is relatively stable in different environmental conditions, and is defined as (Williams et al., 1989),

$$YLD = B_{AG} HI \tag{45}$$

where YLD is the final economic yield (kg ha^{-1}), HI is the harvest index, and B_{AG} is the above-ground biomass, which is equal to total biomass minus root weight (kg ha^{-1}).

Table 1 gives the source or value range of crop parameters in LAWSTAC.

Table 1. The source or value range of crop parameters used in LAWSTAC.

Parameter	Source or Value range
T, RA, LAI_0, H_{max}, RD_{max}, m_r	Provided by the user
T_b, T_0, PHU, BE, LAI_{max}, ah_1, ah_2, L_r, HUI_0, ar_1, ar_2, HI, β	Williams et al. (1989) or Boons-Prins et al. (1993)
K_c	Allen et al., (1998)
h_0, h_1, h_2^L , h_2^H , h_3, r_H, r_L	Wesseling et al. (1991)
EC_{sat}	0~20
EC_{max}	0~40
h_{50}	-2500~-6500 for corn -2500~-7500 for wheat

2.6 Numerical calculation methods

In this model, implicit Euler temporal discretization and cell-centered finite-difference spatial discretization are applied. Although the implicit Euler temporal scheme is questioned about its reliability and efficiency (Clark and Kavetski, 2010), we can improve its stability by iteration and increase efficiency by adjusting the time step. For each grid, RE (Eq. (1)) is discretized as,

$$\frac{\theta_i^{j+1}-\theta_i^j}{\Delta t} = \frac{2}{\Delta z_{i-1}+\Delta z_i}\left[\frac{K_{i+1/2}^{j+1}\left(h_{i+1}^{j+1}-h_i^{j+1}\right)}{\Delta z_i}-\frac{K_{i-1/2}^{j+1}\left(h_i^{j+1}-h_{i-1}^{j+1}\right)}{\Delta z_{i-1}}\right]-\frac{2\left(K_{i+1/2}^{j+1}-K_{i-1/2}^{j+1}\right)}{\Delta z_{i-1}+\Delta z_i}-S_i^j \tag{46}$$

where Δz is the node spacing (cm), Δt is the time step (d), subscript i denotes node number, subscript j denotes time level. Because Eq. (46) includes both θ and h, i.e., it is in "mixed" form. Modified Picard iteration is used to provide the solution in terms of pressure head h (Celia et al., 1990). Let superscript m denote the iteration level, then the implicit Euler temporal discretization is written as,

$$\frac{\theta_i^{j+1,\ m+1}-\theta_i^j}{\Delta t} = \frac{2}{\Delta z_{i-1}+\Delta z_i}\left[\frac{K_{i+1/2}^{j+1,m}\left(h_{i+1}^{j+1,m+1}-h_i^{j+1,m+1}\right)}{\Delta z_i}-\frac{K_{i-1/2}^{j+1,m}\left(h_i^{j+1,m+1}-h_{i-1}^{j+1,m+1}\right)}{\Delta z_{i-1}}\right] -\frac{2\left(K_{i+1/2}^{j+1,m}-K_{i-1/2}^{j+1,m}\right)}{\Delta z_{i-1}+\Delta z_i}-S_i^{j,m} \tag{47}$$

The soil water content and pressure head at the mth iteration, denoted as θ^m and h^m, respectively, are related by,

$$\theta_i^{j+1,m+1}=\theta_i^{j+1,m}+C\left(h_i^{j+1,m}\right)\left(h_i^{j+1,m+1}-h_i^{j+1,m}\right) \tag{48}$$

where C is specific soil water capacity (cm^{-1}). The iteration scheme, Eq. (46), is expressed as,

$$a_i h_{i-1}^{j+1,m+1}+b_i h_i^{j+1,m+1}+e_i h_{i+1}^{j+1,m+1}=f_i,\quad i=1,2,\cdots,M-1 \tag{49}$$

where M is the total number of grid cells in space, and a_i, b_i, e_i, f_i are matrix coefficients at the mth iteration level,

$$a_i = -\frac{2\Delta t}{\Delta z_{i-1}\left(\Delta z_{i-1} + \Delta z_i\right)} K_{i-1/2}^{j+1,m},$$

$$e_i = -\frac{2\Delta t}{\Delta z_i\left(\Delta z_{i-1} + \Delta z_i\right)} K_{i+1/2}^{j+1,m},$$

$$b_i = C_i^{j+1,m} - a_i - e_i,$$

$$f_i = C_i^{j+1,m} h_i^{j+1,m} - \left(\theta_i^{j+1,m} - \theta_i^j\right) - \frac{2\Delta t}{\Delta z_{i-1} + \Delta z_i}\left(K_{i+1/2}^{j+1,m} - K_{i-1/2}^{j+1,m}\right) - S_i^{j,m}\Delta t$$

As demonstrated in Eq. (46), it is necessary to estimate the hydraulic conductivity in the middle of two adjacent nodes. Because hydraulic conductivity is highly nonlinear, various averaging methods for computing $K_{i\pm1/2}$ are available (Srivastava and Guzman-Guzman, 1995; Gastó et al., 2002; Szymkiewicz and Helmig, 2011). It is well known that averaging methods can affect the accuracy, stability and efficiency of the numerical solution (Romano et al., 1998). Here, a range of methods are examined, including,

(1) Arithmetic mean of the conductivity (AC),

$$K_{i\pm1/2} = \frac{K_i + K_{i\pm1}}{2} \tag{50}$$

(2) Geometric mean of the conductivity (GC),

$$K_{i\pm1/2} = \sqrt{K_i K_{i\pm1}} \tag{51}$$

(3) Harmonic mean of the conductivity (HC),

$$K_{i\pm1/2} = \frac{2K_i K_{i\pm1}}{K_i + K_{i\pm1}} \tag{52}$$

(4) Conductivity at the arithmetic mean of pressure head (AP),

$$K_{i\pm1/2} = K\left(\frac{h_i + h_{i\pm1}}{2}\right) \tag{53}$$

(5) Conductivity at the geometric mean of pressure head (GP),

$$K_{i\pm1/2} = K\left(\sqrt{h_i h_{i\pm1}}\right) \tag{54}$$

(6) Conductivity at the harmonic mean of pressure head (HP),

$$K_{i\pm1/2} = K\left(\frac{2h_i h_{i\pm1}}{h_i + h_{i\pm1}}\right) \tag{55}$$

(7) Triadic mean of the conductivity (TC),

$$K_{i\pm1/2} = \frac{K_i + 2K\left(h_{i\pm1/2}\right) + K_{i\pm1}}{4} \tag{56}$$

where $K(h_{i\pm1/2})$ is calculated by Eq.(53).

(8) Conductivity at the higher water pressure node, so-called upstream node (UC) (Srivastava and Guzman-Guzman, 1995),

$$K_{i\pm1/2} = K\left[\max\left(h_i, h_{i\pm1}\right)\right] \tag{57}$$

Among these averaging methods, AC is often used in hydrologic models, e.g., HYDRUS (Simunek et al., 2005).

In this study, the difference scheme for the ADE, Eq. (10), is also implicit Euler temporal discretization and cell-centered finite-difference spatial discretization,

$$A_i c_{i-1}^{j+1} + B_i c_i^{j+1} + E_i c_{i+1}^{j+1} = F_i, \quad i = 1,2,\cdots,M-1 \tag{58}$$

where

$$A_i = -\frac{2\Delta t}{\Delta z_{i-1}\left(\Delta z_{i-1} + \Delta z_i\right)}\left(D_{sh}\right)_{i-1/2}^{j+1} - \frac{\Delta t}{\Delta z_{i-1} + \Delta z_i} q_{i-1}^{j+1},$$

$$B_i = \theta_i^{j+1} + \frac{2\Delta t}{\Delta z_i\left(\Delta z_{i-1} + \Delta z_i\right)}\left(D_{sh}\right)_{i+1/2}^{j+1} + \frac{2\Delta t}{\Delta z_{i-1}\left(\Delta z_{i-1} + \Delta z_i\right)}\left(D_{sh}\right)_{i-1/2}^{j+1},$$

$$E_i = -\frac{2\Delta t}{\Delta z_i\left(\Delta z_{i-1} + \Delta z_i\right)}\left(D_{sh}\right)_{i+1/2}^{j+1} + \frac{\Delta t}{\Delta z_{i-1} + \Delta z_i} q_{i+1}^{j+1},$$

$$F_i = \theta_i^j c_i^j - S_{s,i}^j \Delta t$$

The vertical nodal fluxes, q_i, are computed according to,

$$q_1^{j+1} = -K_{1+1/2}^{j+1}\left(\frac{h_2^{j+1} - h_1^{j+1}}{\Delta z_1} - 1\right) + \frac{\Delta z_1}{2}\left(\frac{\theta_1^{j+1} - \theta_1^j}{\Delta t}\right) \tag{59}$$

$$q_i^{j+1} = \frac{-K_{i+1/2}^{j+1}\left(\frac{h_{i+1}^{j+1} - h_i^{j+1}}{\Delta z_i} - 1\right) - K_{i-1/2}^{j+1}\left(\frac{h_i^{j+1} - h_{i-1}^{j+1}}{\Delta z_{i-1}} - 1\right)}{2}, i = 2,3,\cdots,M \tag{60}$$

$$q_{M+1}^{j+1} = -K_{M+1/2}^{j+1}\left(\frac{h_{M+1}^{j+1} - h_{M}^{j+1}}{\Delta z_M} - 1\right) \tag{61}$$

2.7 Model coupling

Soil water flow, solute transport and crop growth are coupled in LAWSTAC, as shown in the flow chart (Fig. 1).

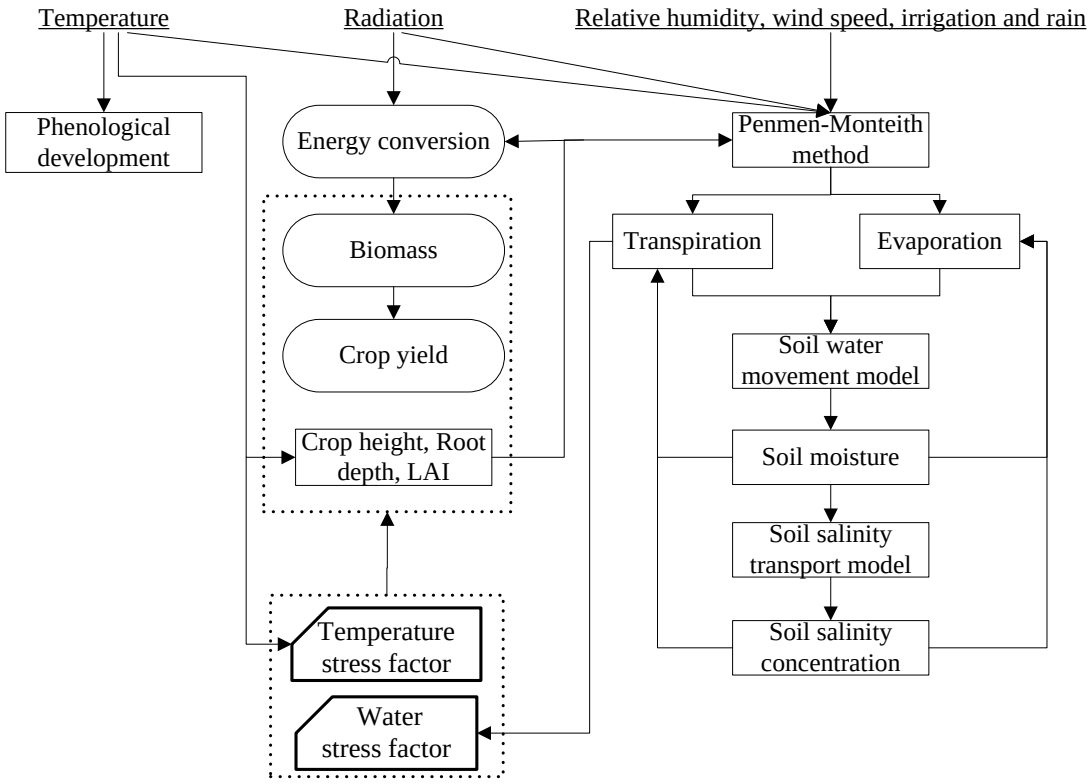

Fig. 1. Flow chart of the coupled model with water flow, solute transport and crop growth model, LAWSTAC.

(1) Potential evapotranspiration is calculated by the Penman-Monteith method, which is partitioned into potential soil evaporation and crop transpiration based on the *LAI* calculated from the crop growth model.

(2) The actual soil evaporation is calculated considering the soil moisture at the ground surface, which is used as the upper boundary condition for the soil water flow model in non-infiltration period. For irrigation or precipitation, the upper boundary is instead switched to the infiltration condition. The actual crop transpiration is assumed

to be equal to the actual root uptake, which is affected by soil moisture and salinity in the root zone and is used as the sink term in the soil water flow model.

(3) The outputs of the soil water flow model are soil moisture as well as flux, which are used to calculate the soil moisture-related parameters and advection term in the soil salinity transport model.

(4) The outputs of the soil solute transport model include the distribution of soil solute concentration in the root zone, which in turn affects the root water uptake.

(5) The ratio between the calculated actual root water uptake and the potential crop transpiration is an indicator of the degree of water stress. Along with temperature stress, water stress modifies crop growth in the crop model.

(6) The crop growth model determines crop height, root length, *LAI*, biomass and yield. These index influence the soil water flow, as described in (1) and (2) above, at the next time step.

3. Evaluation of hydraulic conductivity averaging methods in a layered soil

The eight averaging methods for determining hydraulic conductivity between nodes in LAWSTAC were compared in a layered soil infiltration case (Gastó et al,. 2002). The layered soil structure used for the test case followed Hills et al. (1989). Alternate layers (each 20-cm thick) of Berino loamy fine sand and Glendale clay loam filled the soil domain (total depth of 1 m). The soil hydraulic parameters reported by Hills et al. (1989) are listed in Table 2. The initial condition of soil profile was uniform water pressure head of -10000 cm, and the top boundary condition was constant water pressure head of -50 cm. Fig. 2 shows volumetric water content profiles computed using the various averaging methods after 2 d of infiltration (grid spacing Δz = 2 cm and time increment Δt = 5 s). A fine grid solution (Δz = 0.5 cm, Δt = 5 s) was also calculated (Fig. 2), which closely corresponds to the reference solution (Gastó et al., 2002) and is found to be negligibly affected by the choice of hydraulic conductivity averaging methods. Considering the location of the wetting front shown in Fig. 2, the arithmetic mean (AC), geometric mean (GC), geometric mean of pressure head (GP), harmonic mean of pressure head (HP), triadic mean (TC) and

upstream node (UC) lead to an overestimation of the internodal conductivity, while the harmonic mean (HC) and arithmetic mean of pressure head (AP) underestimate it. Among the averaging methods, the HC has the lowest calculated value of hydraulic conductivity, which is inappropriate for simulating unsaturated flow (Schnabel and Richie, 1984). Overall, the AC, GC and TC methods have smaller errors in simulating water movement in layered soil, with the mean relative errors of 4.4%, 3.8% and 5.2% compared to the fine grid solution, respectively. Thus, the AC, GC and TC methods are more suitable for water infiltration simulation in layered soil under the implicit Euler temporal scheme.

To further assess the AC, GC and TC procedures of the LAWSTAC in multilayered soil (more than 10 layers), a lysimeter infiltration experiment of Hills et al. (1989) was selected. The lysimeter (94.7-cm diameter, 610-cm long) was filled with alternating layers of Berino loamy fine sand and Glendale clay loam. The soil core had 29 layers with a total depth of 585 cm. The soil hydraulic parameters measured by Hills et al. (1989) are listed in Table 2. The initial soil water contents were 0.029 $cm^3\ cm^{-3}$ for the sand and 0.107 $cm^3\ cm^{-3}$ for the clay loam. The infiltration water flux applied to the lysimeter was 2.314 cm d^{-1}. Fig. 3 shows the simulated and observed soil water content profiles after 56 days of infiltration into the layered lysimeter. The AC, GC and TC methods all predicted the soil water content well in the clay loam layers and slightly overestimated it in the sand layers for grid spacing of 1 cm and 4 cm, which closely corresponds to the reference solution simulated by Hills et al. (1989). For the coarse grid (Δz = 4 cm), the infiltration wetting fronts simulated by the AC, GC and TC methods are slightly deeper than the reference solution, but the three averaging methods remain accuracy in simulating water content in the soil profile (Fig. 3b). Moreover, the coarse space discretization can improve simulation efficiency by reducing the computational time compared the fine grid, especially for the GC method (Fig. 4). Therefore, for water flow in a multilayered soil with long buried depth, coarse space discretization is permitted for AC, GC and TC methods without causing larger errors in simulation under the implicit Euler temporal

scheme.

Table 2. Soil hydraulic parameters used for the comparison of eight hydraulic conductivity averaging methods.

Soil	θ_r ($cm^3\ cm^{-3}$)	θ_s ($cm^3\ cm^{-3}$)	α (cm^{-1})	n	l	K_s ($cm\ d^{-1}$)
Berino loamy fine sand	0.0286	0.3658	0.028	2.239	0.5	541
Glendale clay loam	0.106	0.4686	0.0104	1.3954	0.5	13.1

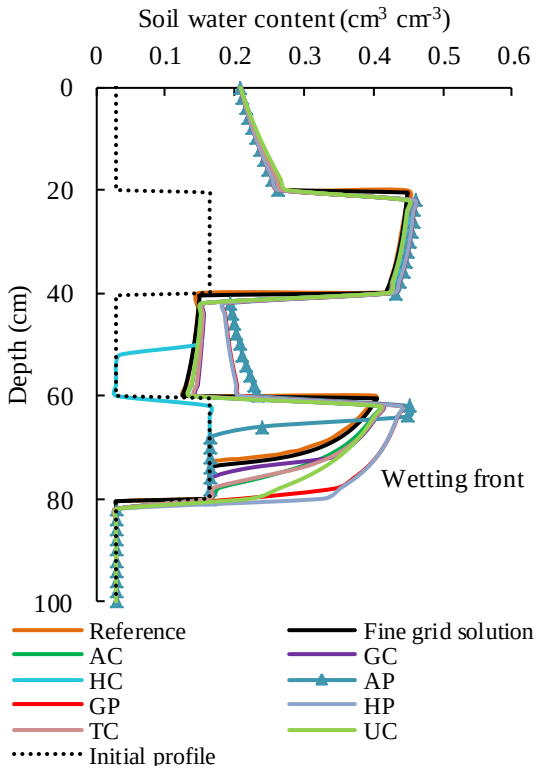

Fig. 2. Volumetric water content profile in a layered soil. Comparison of results from various averaging methods with a fine grid solution for the case of constant surface pressure head infiltration.

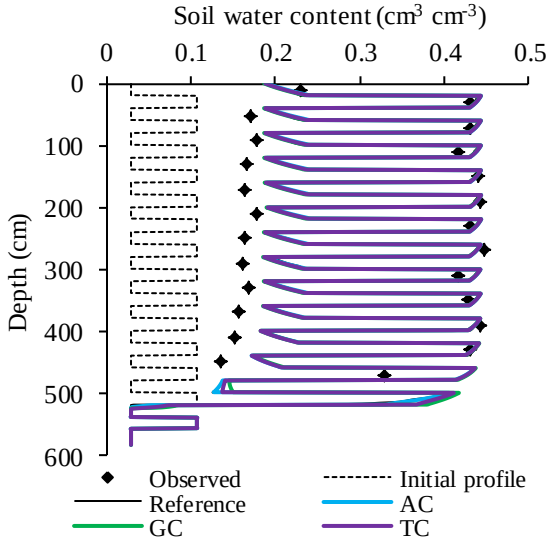

(a)

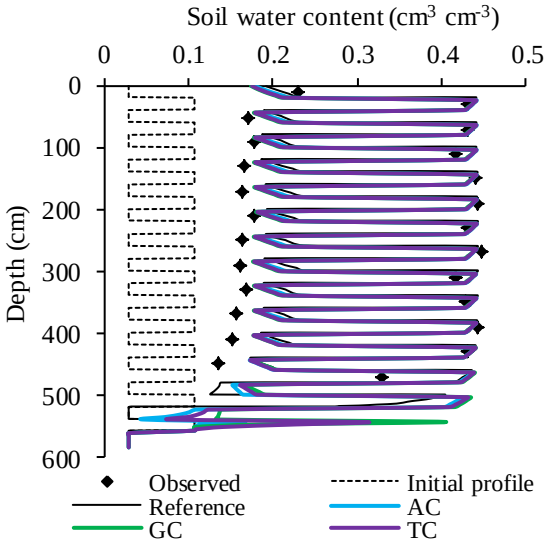

(b)

Fig. 3. Volumetric soil water content profiles in a multilayered soil after 56 days of infiltration under a constant surface water flux. Comparison of the observations and simulation results based on the arithmetic mean (AC), geometric mean (GC) and triadic mean (TC) with Δz = 1 cm (a) and 4 cm (b).

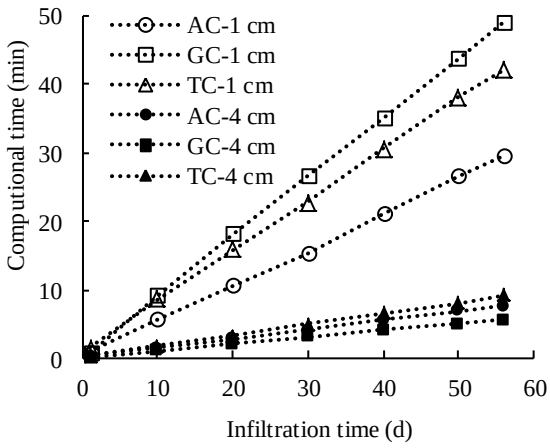

Fig. 4. Computational time for the arithmetic mean (AC), geometric mean (GC) and triadic mean (TC) with Δz = 1 cm and 4 cm.

4. Evaluation of LWASTAC based on and model comparisons in a field condition

4.1 Brief introduction of the models used for evaluation of LAWSTAC

In order to assess the performance of the LAWSTAC model in a field condition, two widely used hydrologic models, HYDRUS-1D (Simunek et al., 2005) and SWAP (van Dam et al., 1997), were selected for simulating soil water-solute dynamics and crop growth processes. The models were chosen for the following reasons. First, soil water flow and solute transport simulations in the three models are all based on the RE and ADE, respectively. Second, for the method of calculation of actual root water uptake, the Feddes model can be used in all models. Finally, all these models can be applied to layered soils. The detailed algorithm and structure of the three models are listed in Table 3.

Table 3. Algorithm and structure of the SWAP, HYDRUS-1D and LAWSTAC.

Items	Contents	SWAP	HYDRUS-1D	LAWSTAC
Numerical algorithm	Soil water	Implicit FD	Implicit FE	Implicit FD
	Solute	Explicit FD	Implicit FE	Implicit FD
Soil water flow	Layers	10	> 10	> 10
	K averaging method	2	1	8
	Root water uptake	Y	Y	Y
Solute transport	Layers	10	> 10	> 10
	Root adsorption	Y	Y	Y
Crop growth	Leaf area index	Y	N	Y
	Crop height	Y	N	Y
	Biomass	Y	N	Y
	Yield	Y	N	Y
	Root development	Y	N	Y
	Actual transpiration	Y	Y	Y
	Photosynthesis	Y	N	N

Respiration	Y	N	N

Note: FD denotes finite difference, FE denotes finite element, Y denotes yes, and N denotes no.4.2 Scenario and parameters used for evaluation

For model comparison, we selected a simulation case based on a wheat growing experiment conducted at the Huinong experimental site, located in Ningxia Autonomous Region, Northwest China (106°39′ E, 39°04′N), with water flow and solute transport in the layered root zone during 2007 and 2008. The climate in the region is arid continental with annual rainfall of 180-200 mm. Spring wheat was sown on March 16 and harvested on July 11. The crop was irrigated with water diverted from the Yellow River. Irrigation depths and times are shown in Table 4. The groundwater lever was shallow with depth of 0.5-2.5 m. The total dissolved solid concentration of the irrigation water and groundwater averaged 0.47 and 1.2 g L^{-1}, respectively. The soil profile at the experimental site has various horizontal layers and the physical properties are shown in Table -5. The detailed experimental scheme can be referred to Xu et al. (2013). The available data were soil water and salt contents in different depths, leaf area index, and dry grain yield.

Table 4. Irrigation scheduling of spring wheat for 2007 and 2008.

Year	Date (d/m)	Irrigation depth (mm)	Year	Date (d/m)	Irrigation depth (mm)
2007	3/5	135	2008	3/5	135
	24/5	90		24/5	90
	6/7	90		29/6	90

Table 5. Measured soil physical properties at the experimental site.

Soil layer (cm)	Clay (%)	Silt (%)	Sand (%)	Soil texture	Bulk density (g cm^{-3})	Field capacity (cm^3 cm^{-3})
0-30	4.8	39.3	55.6	Sandy loam	1.41	0.28
30-81	5.0	41.0	54.0	Loam	1.60	0.31
81-103	3.7	41.3	55.0	Loam	1.52	0.28
103-140	3.8	74.7	21.5	Silty loam	1.55	0.36

>140	2.0	27.0	74.0	Sandy loam	1.58	0.32

4. 3 Model inputs

To make the results simulated by the three models comparable, we kept the initial input data consistent to the extent feasible. In simulating soil water and salinity dynamics, we input the same soil hydraulic parameters and solute transport parameters. To make sure the three models have the same atmospheric evaporation capacity, all three models used the reference evapotranspiration and crop coefficient to calculate the potential crop transpiration. For root growth, as SWAP assumes the root length develops linearly with time, the root growth in the other two models was adjusted accordingly. For the root distribution with soil depth, when the root length changes with time, only the function of Hoffman and van Genuchten, Eq. (24), can be used to describe the root spatial distribution in HYDRUS-1D, so the other two models used the same function. The Feddes model was used to calculate the root water uptake under water and salinity stresses in the three models. In partitioning evapotranspiration into evaporation and transpiration, *LAI* values are necessary for all models, but HYDRUS-1D cannot simulate leaf area changes, so the *LAI* values used in HYDRUS-1D were calculated by taking the average *LAI* values simulated by SWAP and LAWSTAC. The three models all used the arithmetic mean conductivity, AC, given by Eq. (50). The upper boundary condition was set to the atmospheric boundary condition since the soil surface was open to the atmosphere and was shifted to infiltration when rainfall or irrigation occurred. A variable pressure head boundary condition was specified at the bottom due to the high groundwater table.

The crop growth modules in LAWSTAC and in SWAP (detailed crop model) both depend on temperature and intercepted radiation to determine phenological development and biomass accumulation, although the approaches are slightly different. For example, SWAP simulates crop development from emergence to maturity and uses photosynthesis and respiration to calculate biomass, while LAWSTAC calculates the crop development stage from sowing to maturity and uses a

crop parameter to convert radiation to biomass. Nevertheless, the driving mechanisms of crop growth in the two models are similar.

Input parameters for SWAP, HYDRUS-1D and LAWSTAC are shown in Table 6. The crop growth indicators, including maximum crop height, maximum root depth, and maximum *LAI*, were determined according to measured values. Empirical parameters such as the extinction coefficient were selected by referring to the literature (Williams et al., 1989; Boons-Prins et al., 1993). The hydraulic parameters and solute transport parameters of the layered soil used in the three models are listed in Table 7.

The input parameters of the three models for soil water flow, solute transport and crop growth were calibrated (via least squares minimization) using the observed data in 2007, including the soil water contents and salt concentrations in each soil layer, *LAI* and yield. The calibrated models were validated using experiment data from the 2008 growing season.

4.4 Evaluation of model outputs

Model performance was evaluated by comparing the observed values with the simulated results using different criteria, viz., the root mean square error (*RMSE*), and the mean relative error (*MRE*). These metrics are defined, respectively, as follows,

$$RMSE = \sqrt{\frac{1}{N}\sum_{i=1}^{N}\left(P_i - O_i\right)^2} \tag{62}$$

$$MRE = \frac{1}{N}\sum_{i=1}^{N}\frac{\left(P_i - O_i\right)}{O_i}\times 100\% \tag{63}$$

where P_i and O_i (i=1, 2,……，N) are, respectively, the simulated and observed values, and N is the number of observations.

The model performance comparison penalized by the number of calibrated parameters was quantified by the Akaike information criterion (*AIC*; Akaike, 1973),

$$AIC = 2k_p + n_s \ln\left(\frac{RSS}{n_s}\right) \tag{64}$$

where k_p is the number of calibrated parameters in the model, n_s is the sample size, and RSS is the residual sum of squares.

Table 6. Parameters and their values used in the SWAP, HYDRUS-1D and LAWSTAC.

Parameter	Definition	Value
General		
θ_r	Residual water content (cm^3 cm^{-3})	Table 7
θ_s	Saturated water content (cm^3 cm^{-3})	Table 7
K_s	Saturated hydraulic conductivity (cm d^{-1})	Table 7
α	Air-entry parameter in Eq. (2)	Table 7
l	Pore connectivity/tortuosity parameter in Eq. (4)	Table 7
n	Pore size distribution parameter in Eq. (2)	Table 7
D_L	Longitudinal dispersivity (cm)	Table 7
D_0	Molecular diffusion coefficient in free water (cm^2 d^{-1})	Table 7
L_c	Length of crop (wheat) cycle (d)	118
T_b	Minimum temperature for plant growth (°C)	2
T_0	Optimal temperature for plant growth (°C)	20
h_{max}	Maximum crop height (cm)	96
RD_{max}	Maximum root length (cm)	100
h_0	Anaerobiosis point (cm)	-0.1
h_1	*h* below which roots uptake water at the maximum possible rate (cm)	-1
h_2^H	Maximal *h* below which roots can no longer uptake water at the maximum rate (cm)	-500
h_2^L	Minimal *h* below which roots can no longer uptake water at the maximum rate (cm)	-900
h_3	Wilting point pressure head (cm)	-16000
r_H	Potential transpiration rate in Eq. (29) (cm d^{-1})	0.5
r_L	Potential transpiration rate in Eq. (29) (cm d^{-1})	0.1
SWAP		
*TSUM*1	Temperature sum from emergence to anthesis (°C)	857.0
*TSUM*2	Temperature sum from anthesis to maturity (°C)	737.0
RGRLAI	Maximum relative increase in *LAI* (m^2 m^{-2} d^{-1})	0.01
LAIEM	Leaf area index at emergence (m^2 m^{-2})	0.02
SPAN	Life span of leaves under optimum conditions (d)	14.5
LT	Lower threshold temperature for ageing of leaves (°C)	1.5
IDW	Initial total crop dry weight (kg ha^{-1})	40.0
AMAX	Maximum leaf CO_2 assimilation rate at development stage of crop growth (kg ha^{-1} h^{-1})	40.0
EFFTB	Light-use efficiency of assimilation of single leave (kg ha^{-1} h^{-1} J^{-1} m^{-2} s^{-1})	0.55
KDIR	Extinction coefficient for direct visible light (-)	0.55
KDIF	Extinction coefficient for diffused visible light (-)	1.0
CVO	Conversion efficiency of assimilates into storage organ (kg kg^{-1})	0.89
CVS	Conversion efficiency of assimilates into stem (kg kg^{-1})	0.74
CVL	Conversion efficiency of assimilates into leaf (kg kg^{-1})	0.70

CVR	Conversion efficiency of assimilates into root (kg kg^{-1})	0.75
RMO	Relative maintenance respiration rate of storage organs (kg CH_2O kg^{-1} d^{-1})	0.003
RMS	Relative maintenance respiration rate of stems (kg CH_2O kg^{-1} d^{-1})	0.015
RML	Relative maintenance respiration rate of roots (kg CH_2O kg^{-1} d^{-1})	0.01
RMR	Relative maintenance respiration rate of leaves (kg CH_2O kg^{-1} d^{-1})	0.02
*Q*10	Relative change in respiration rate per 10°C temperature change	2.0
PERDL	Maximum relative death rate of leaves due to water stress (d^{-1})	0.01
RRI	Maximum daily increase in root length (cm d^{-1})	1.3
RDI	Initial root length (cm)	5
PIC	Precipitation interception coefficient (-)	0.25
EC_{sat}	Salinity threshold below which no salt stress (dS m^{-1})	6
EC_{slop}	Decline rate of root water uptake (% m dS^{-1})	4
HYDRUS-1D		
β	extinction coefficient (-)	0.55
Threshold	Salinity threshold below which no salt stress (dS m^{-1})	12
slop	Decline rate of root water uptake (% m dS^{-1})	2
Ose.Coeff.	Coefficients to transform concentrations into equivalent osmotic pressure heads	1.9
hCritA	Value of the minimum allowed pressure head at the soil surface (cm)	10000
LAWSTAC		
BE	Plant radiation-use efficiency ((kg m^2 ha^{-1} MJ^{-1})	29
LAI_{max}	Potential maximum leaf area index (-)	7.1
LAI_0	Actural maximum leaf area index (-)	5.7
HUI_0	Fraction of growing season controlled by cumulative temperature when leaf area index starts declining (-)	0.5
ah_1	Crop parameters in Eq. (39)	10.02
ah_2	Crop parameters in Eq. (39)	50.95
β	extinction coefficient (-)	0.55
Lr	*LAI* decline rate (-)	1.8
HI	Harvest index (-)	0.46
PHU	Required cumulative heat unit for maturity (°C)	1800
EC_{sat}	Salinity threshold below which no salt stress (dS m^{-1})	6
EC_{slop}	Decline rate of root water uptake (% m dS^{-1})	4

Table 7. Soil hydraulic parameters and salt transport parameters used in the three models.

Depth (cm)	θ_r (cm^3 cm^{-3})	θ_s (cm^3 cm^{-3})	α (cm^{-1})	n	l	K_s (cm d^{-1})	D_L (cm)	D_0 (cm^2 d^{-1})
0-30	0.02	0.40	0.02	1.35	0.5	14	20	5.5
30-81	0.02	0.41	0.015	1.39	0.5	13		

81-103	0.01	0.38	0.018	1.35	0.5	10
103-140	0.01	0.45	0.013	1.26	0.5	7
>140	0.01	0.41	0.02	1.25	0.5	10

4.5 Comparison of simulation results

Model comparisons included simulated evapotranspiration, soil water content, soil salinity and crop growth indicators. The aboveground crop growth processes were compared only for SWAP and LAWSTAC as HYDRUS-1D does not simulate these. The comparisons are shown in Figs. 5-8.

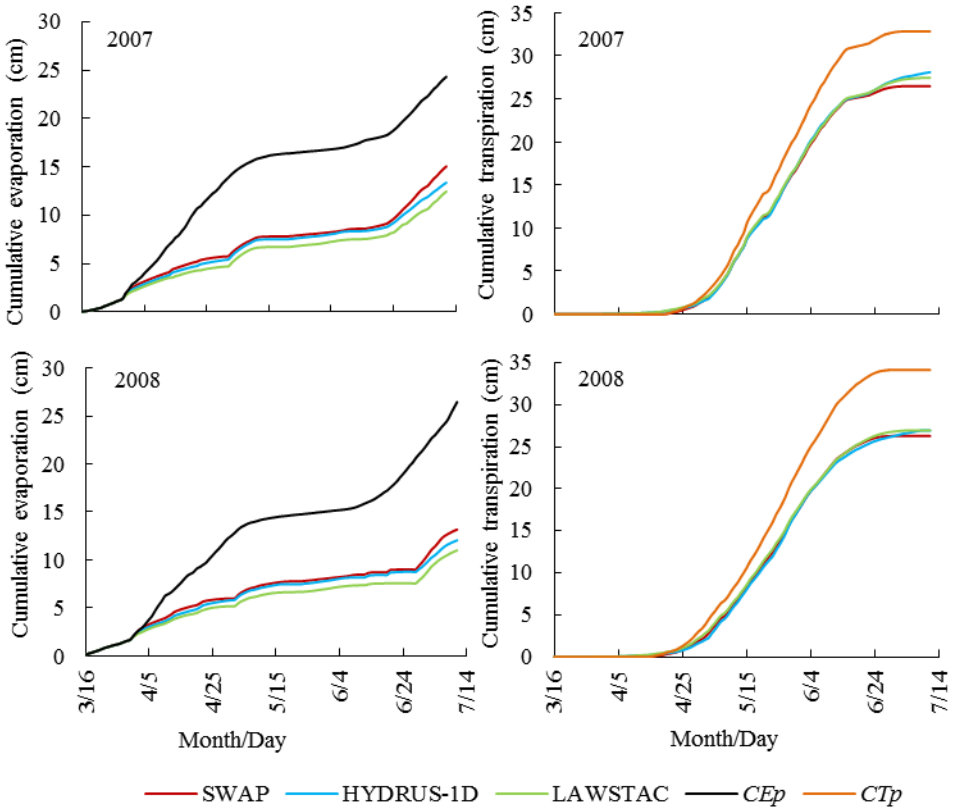

(a) (b)

Fig. 5. Comparison of simulated results of cumulative evaporation (a) and transpiration (b) by the three models in 2007 and 2008. Note: *CEp* and *CTp* are cumulative potential evaporation and transpiration, respectively.

4.5.1 Actual crop transpiration and soil evaporation

Fig. 5 reveals several differences between the models in simulating cumulative actual soil evaporation and crop transpiration in 2007 and 2008. Fig. 5a shows that results for cumulative actual soil evaporation have similar trends, although values vary somewhat. SWAP has the highest actual evaporation rates of the three models, while the rates for LAWSTAC are the lowest. For HYDRUS-1D, when the pressure head in the soil surface is higher than the critical value, the actual evaporation rate is equal to the potential evaporation rate. Otherwise, when the surface pressure head drops below the critical value, evaporation is calculated through Darcy's law (Ma et al., 2011). In SWAP, the actual evaporation rate is determined by taking the minimum value of the potential evaporation rate and the Darcy flux. The actual evaporation computed by LAWSTAC is based on the three-stage evaporation process, Eq. (22).

Fig. 5b shows that the actual crop transpiration rates simulated by the three models are similar. The actual transpiration is the product of potential transpiration and the water stress coefficient as calculated by Feddes model in the three models, so the differences of the actual transpiration simulated by the three models are small.

4.5.2 Soil water content

The observed soil water contents and the simulated values by SWAP, HYDRUS-1D and LAWSTAC during calibration and validation are shown in Figs. 6 and 7 (left). The three models show little difference in simulating soil water flow, and they can capture both the values and variations of measured soil water contents for various soil layers. Though the numerical schemes for solving the Richards equation are different in the three models (finite element scheme for HYDRUS-1D, finite difference scheme for SWAP and LAWSTAC), they are all in fully implicit scheme which can improve convergence in iteration (Celia et al. 1990). Therefore, the three models all can obtain the numerical solution of the soil water flow that satisfies the tolerance through iteration.

The performance of the three models was also assessed quantitatively. The

values of *RMSE* and *MRE* for soil water contents in the whole soil profile are shown in Table 9. The *RMSE* values of the three models were all 0.02 cm^3 cm^{-3} and 0.06 cm^3 cm^{-3} during the calibration and validation, respectively, and the *MRE* values were less than 0.91% and 8.21% for the calibration and validation, respectively. The results show that three models predict the soil water contents well in the field condition.

4.5.3 Soil salinity concentration

The soil salinity concentration in various soil layers are shown in Figs. 6 and 7 (right), where the three models simulate the soil salinity in different depths well compared with the observed values over the wheat growing season of 2007 and 2008. The simulated results by the three models have no significant difference except a little fluctuation for SWAP in salt simulation in the surface soil. This is because of the different numerical schemes used in the three models. For solute transport simulation, an implicit temporal discretization was used by HYDRUS-1D and LAWSTAC, while SWAP used an explicit temporal discretization. Though the SWAP ran the soil salinity simulation in this simulation case successfully, the explicit scheme it used may have some stability problems for some distinctly layered soil (fine grid needed) due to the time step required to satisfy the stability criterion.

The fitness indicators of soil salinity concentration by the three models are given in Table 9. Results show that the *RMSE* values of the SWAP, HYDRUS-1D and LAWSTAC are among 1.59 ~ 3.73 g L^{-1} and the respective *MRE* values are among -4.41% ~ 1.40% for the calibration and validation, which demonstrates that the results of simulated salinity are still satisfactory.

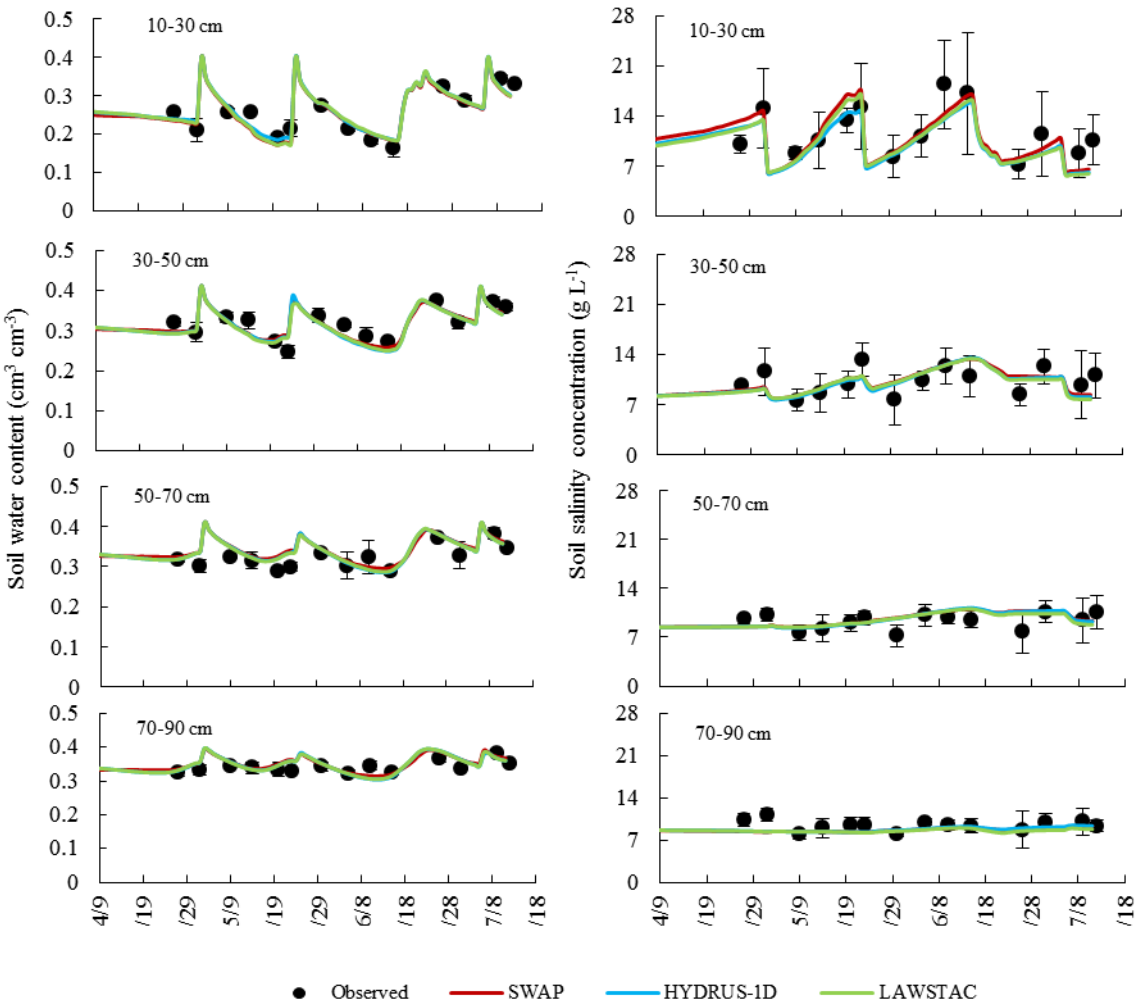

Fig. 6. Comparison of simulated soil water content (left) and soil salinity (right) in different soil layers by the three models – results for calibration year 2007.

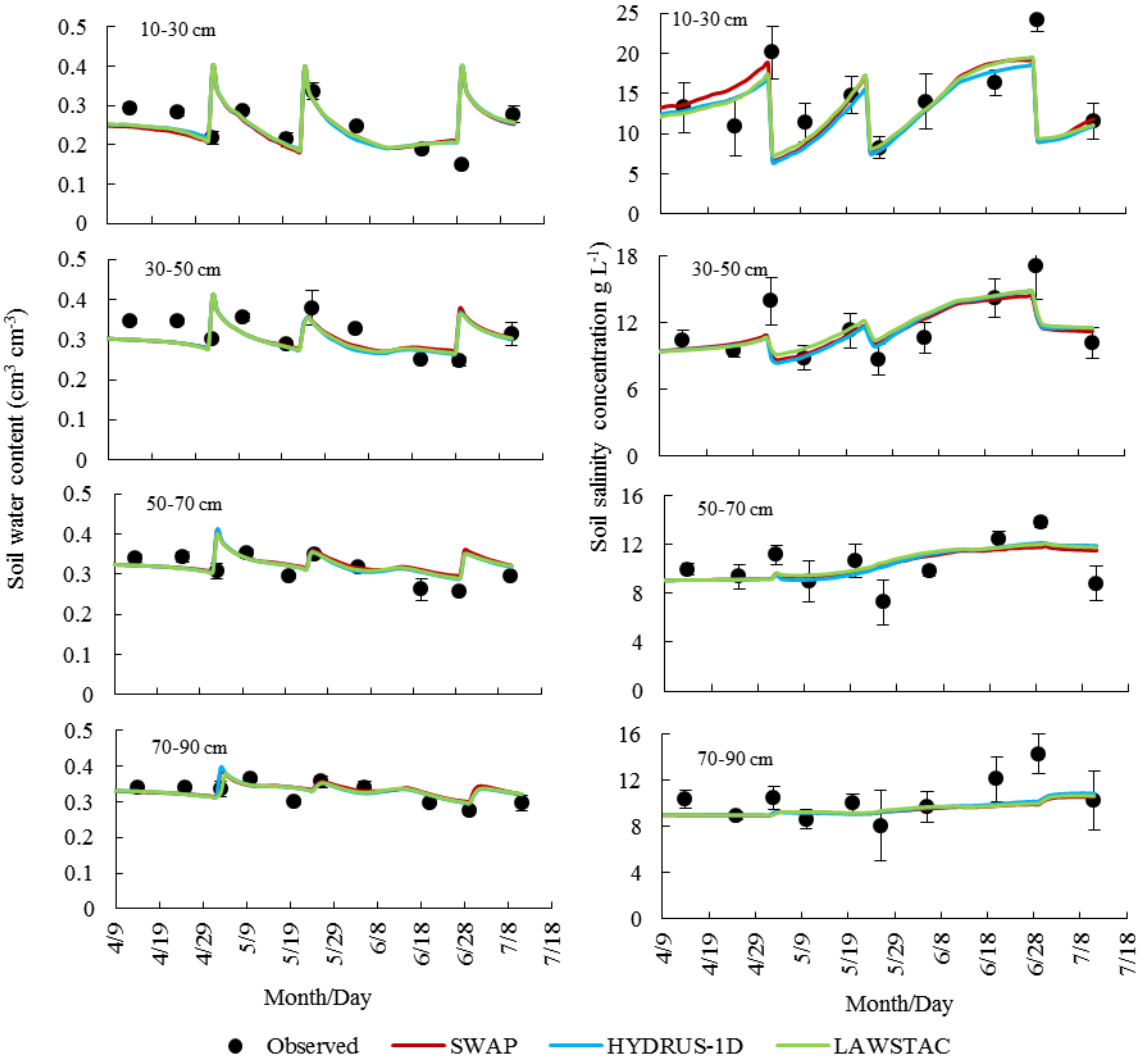

Fig. 7. Comparison of simulated soil water content (left) and soil salinity (right) in different soil layers by the three models for the validation year 2008 data.

4.5.4 *LAI*, biomass and crop yield

Aboveground crop growth, as explained earlier, could only be simulated by SWAP and LAWSTAC. Results for *LAI* and biomass are presented in Fig. 8. The SWAP and LAWSTAC both simulate crop growth using the incoming photo-synthetically active radiation absorbed by the crop canopy. However, SWAP considers crop photosynthesis and respiration, which is more complex than LAWSTEC in terms of mechanism (Singh et al., 2006). From Fig. 8, we can see that

despite this, LAWSTAC give the reasonable results for the evolution of *LAI* and biomass compared with SWAP. For leaf area index, the deviations were considered acceptable for the two models (SWAP: 0.43 < *RMSE* < 0.46, 3.88% < *MRE* < 14.86%; LAWSTAC: 0.29 < *RMSE* < 0.43, -0.27% < *MRE* < 13.57%). The lager mean relative error, *MRE*, for validation is due to less measured *LAI* data in 2008.

The simulated crop yield by SWAP (4610 kg ha^{-1}) and LAWSTAC (4619 kg ha^{-1}) are only slightly higher than the observed yield (4600 kg ha^{-1}) during the calibration. The observed crop yield was 4771 kg ha^{-1} for 2008 and the simulated yields by SWAP and LAWSTAC were 4423 kg ha^{-1} and 4372 kg ha^{-1} during the validation, respectively, thus showing a small difference only. The results indicate that the LAWSTAC model can be used to estimate agricultural production.

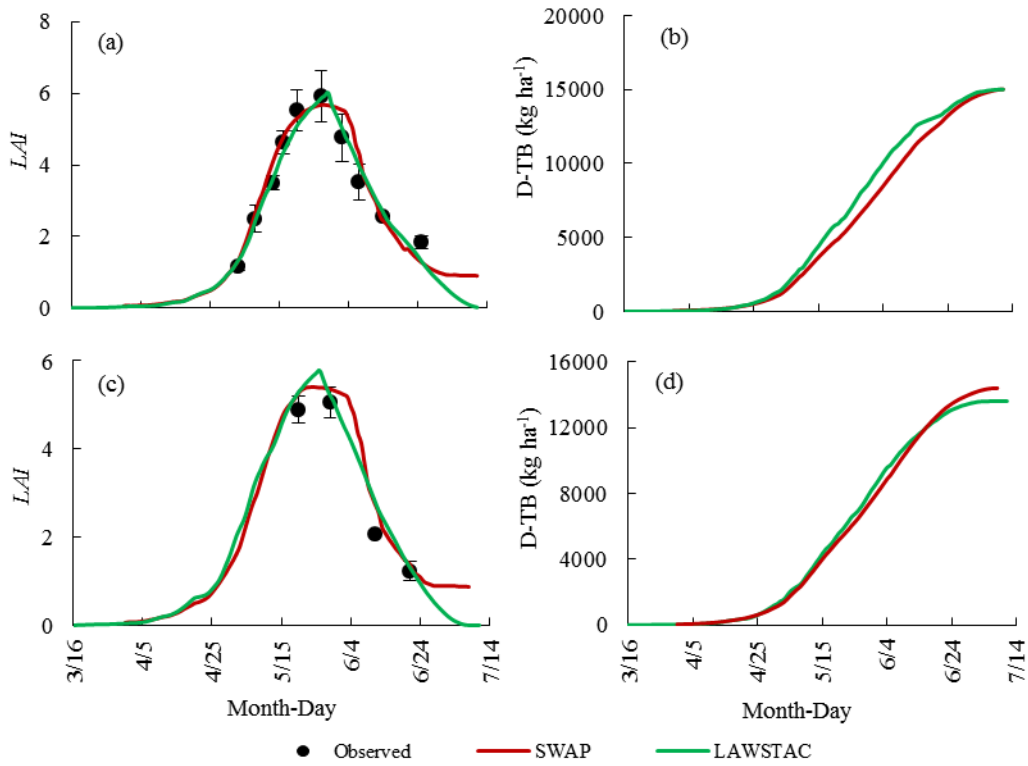

Fig. 8. Comparison of simulated leaf area index (*LAI*, a and c) and dry total biomass (D-TB, b and d) by SWAP and LAWSTAC during model calibration (a and b) and validation (c and d).

4.5.5 Model performance comparison

The model performance comparison was conducted only for SWAP and LAWSTAC as HYDRUS-1D is not suitable for crop simulation. The total calibrated parameters in SWAP and LAWSTAC were 84 and 54, respectively. As shown in Table 8, the *AIC* values for soil water content, soil salinity and leaf area index simulated by SWAP are all larger than that simulated by LAWSTAC, which indicates the LAWSTAC is more efficient than SWAP.

Table 8. Model comparison: Akaike information criterion (*AIC*) for soil water content, soil salinity and leaf area index.

Year	Model	Soil water content	Soil salinity	Leaf area index
2007	SWAP	-229.8	219.1	152.3
	LAWSTAC	-289.9	159.7	84.7
2008	SWAP	-51.2	273.3	161.2
	LAWSTAC	-114.0	209.6	88.2

Table 9. Goodness-of-fit indicators of soil water content, soil salinity concentration and *LAI* for model calibration and validation.

	Models	Items	Mean relative error, *MRE* (%)	Root mean square error, *RMSE*, (cm^3 cm^{-3} or g L^{-1})
Calibration (2007)	SWAP	Soil water content	0.91	0.02
		Soil salinity concentration	1.40	1.63
		LAI	3.88	0.46
	HYDRUS-1D	Soil water content	0.67	0.02
		Soil salinity concentration	-0.86	1.59
	LAWSTAC	Soil water content	0.28	0.02
		Soil salinity concentration	-0.89	1.64
		LAI	-0.27	0.29
Validation (2008)	SWAP	Soil water content	8.21	0.06
		Soil salinity concentration	-3.43	3.73
		LAI	14.86	0.43
	HYDRUS-1D	Soil water content	7.68	0.06
		Soil salinity concentration	-4.41	3.72
	LAWSTAC	Soil water content	7.31	0.06
		Soil salinity concentration	-2.57	3.56
		LAI	13.57	0.43

5. Conclusions

In this study, a new coupled hydrology-crop growth model, LAWSTAC, was developed based on Richards equation for soil water flow, the advection-dispersion equation for solute transport, as well as a detailed crop growth model. LAWSTAC considers the soil vertical heterogeneity in simulating water-solute dynamics in the root zone as well as crop growth. The interaction of crop growth and soil water

flow/solute transport was improved by integration of two different root water uptake models (Feddes and S-shaped). LAWSTAC provides eight different hydraulic conductivity internodal averaging methods to account for abrupt variations at the interfaces of soil layers. Numerical testing showed that the model can be used into multilayered soils, and the internodal conductivity computed using the arithmetic mean (AC), the geometric mean (GC) or the triadic mean (TC) were suitable for simulating water infiltration in layered soil.

LAWSTAC was assessed by comparing its simulation results with the other two widely used models, HYDRUS-1D and SWAP. The three models were calibrated and validated for prediction of soil water and salt dynamics, and growth of spring wheat based on experimental data from 2007 (calibration year) and 2008 (validation year) in an experimental station in Northwest China. Under the same scenario, the three models performed almost the same in simulating soil water contents in different soil layers, while LAWSTAC and HYDRUS-1D, in contrast to SWAP, simulated the soil salinity dynamics more consistently and stably. In terms of crop growth simulation, although LAWSTAC requires fewer crop data inputs, it was found to perform reasonable compared with the more complex SWAP model. Therefore, the LAWSTAC can be used for simulating soil water and salt dynamics, and crop growth processes in layered-soil farmland. Note that we have tested LAWSTAC with two years of field data in the arid region of Northwest China. In future study, the model needs to be tested by more data under different climate and soil conditions.

Acknowledgement

This work was supported by the National Key R&D Program (2016YFC040106), National Natural Science Foundation of China (51379207, 91425302), and the Program of Introducing Talents of Discipline to Universities (Grant No. B14002).

References

Akaike, H., 1973. Information theory and an extension of the maximum likelihood principle. Pages 267–281 in B. N. Petrov and S. Caski, editors. Proceedings of the Second International Symposium on Information Theory. Akademiai Kaido, Budapest, Hungary. https://link.springer.com/chapter/10.1007%2F978-1-4612-1694-0_15 (last accessed 22 August 2018).

Allen, R.G., Pereira, L.S., Raes, D., Smith, M., 1998. Crop evapotranspiration-guidelines for computing crop water requirements-FAO Irrigation and drainage paper 56. Food and Agriculture Organization of the UN, Rome, Italy. http://www.hidmet.gov.rs/podaci/agro/table%20of%20contens_files.pdf (last accessed 22 August 2018).

An, H., Noh, S.J., 2014. High-order averaging method of hydraulic conductivity for accurate soil moisture modeling. J. Hydrol. 516(4), 119-130. DOI: 10.1016/j.jhydrol.2013.12.032.

Bear, J., 1972. Dynamics of fluids in porous media. American Elsevier, New York, NY, USA, 764 pp. http://tocs.ulb.tu-darmstadt.de/10865209.pdf (last accessed 22 August 2018).

Boogaard, H.L., Van Diepen, C.A., Rötter, R.P., Cabrera, J.M.C.A., Van Laar, H.H., 1998. WOFOST 7.1: User's guide for the WOFOST 7.1 crop growth simulation model and WOFOST control center 1.5. DLO Winand Staring Centre, Wageningen, Netherlands. http://www.06climate.com/data/JK82mxJBHsrAsdHqQvsK/ewiosnlaslkal/public/agrometeorology/crop%20model/wofost%2071%20system%20explain.pdf (last accessed 22 August 2018).

Boons-Prins, E.R., de Koning, G.H.J., van Diepen, C.A., Penning de Vries, F.W.T., 1993. Crop specific simulation parameters for yield forecasting across the European Community. Simulation Reports CABO-TT 32. DLO Winand Staring Centre, Wageningen, Netherlands. http://edepot.wur.nl/308997 (last accessed 22 August 2018).

Cameira, M.R., Ahuja, L., Fernando, R.M., Pereira, L.S., 2000. Evaluating field measured soil hydraulic properties in water transport simulations using the RZWQM. J. Hydrol. 236(1), 78-90. DOI: 10.1016/S0022-1694(00)00286-9.

Celia, M.A., Bouloutas, E.T., Zarba, R.L., 1990. A general mass-conservative numerical solution for the unsaturated flow equation. Water Resour. Res. 26(7), 1483-1496. DOI: 10.1029/WR026i007p01483.

Childs, S.W., Hanks, R.J., 1975. Model of soil salinity effects on crop growth. Soil Sci. Soc. Am. J. 39(4), 617-622. DOI: 10.2136/sssaj1975.03615995003900040016x.

Clark, M. P., Kavetski, D., 2010. The ancient numerical demons of conceptual hydrological modeling: 1. Fidelity and efficiency of time stepping schemes. Water Resour. Res. 46(10), 5613-5618. DOI: 10.1029/2009WR008894.

Cominelli, E., Conti, L., Tonelli, C., Galbiati, M., 2013. Challenges and perspectives to improve crop drought and salinity tolerance. New Biotechnol. 30(4), 355-361. DOI: 10.1016/j.nbt.2012.11.001

Eitzinger, J., Trnka, M., Hosch, J., Zalud, Z., Dubrovsky, M., 2004. Comparison of CERES, WOFOST and SWAP models in simulating soil water content during growing season under different soil conditions. Ecol. Model. 171(3), 223-246. DOI: 10.1016/j.ecolmodel.2003.08.012.

Feddes, R.A., Bresler, E., Neuman, S.P., 1974. Field test of a modified numerical model for water uptake by root systems. Water Resour. Res. 10(6), 1199-1206. DOI: 10.1029/WR010i006p01199.

Gastó, J.M., Grifoll, J., Cohen, Y., 2002. Estimation of internodal permeabilities for numerical simulation of unsaturated flows. Water Resour. Res. 38(12), 1326. DOI: 10.1029/2002WR001529.

Hanson, J.D., Ahuja, L.R., Shaffer, M.D., Rojas, K.W., DeCoursey, D.G., Farahani, H., Johnson, K., 1998. RZWQM: Simulating the effects of management on water quality and crop production. Agric. Syst. 57(2), 161-195. DOI: 10.1016/S0308-521X(98)00002-X.

Hills, R.G., Porro, I., Hudson, D.B., Wierenga, P.J., 1989. Modeling one-dimensional infiltration into very dry soils, 1, Model development and evaluation. Water Resour. Res., 25(6), 1259-1269. DOI: 10.1029/WR025i006p01259.

Hills, R.G., Hudson, D.B., Porro, I., Wierenga, P.J., 1989. Modeling one-dimensional infiltration into very dry soils, 2, Estimation of the soil water parameter and model predictions. Water Resour. Res., 25(6), 1271-1282. DOI: 10.1029/WR025i006p01271.

Hoffman, G.J., van Genuchten, M.Th., 1983. Soil properties and efficient water use: Water management for salinity control. Limitations and efficient water use in crop production, American Society of Agronomy, Madison, WI, USA, pp. 73-85. https://www.ars.usda.gov/ARSUserFiles/20360500/pdf_pubs/P0701.pdf (last accessed 22 August 2018).

Hutson, J. L., Wagenet, R. J., 1990. An overview of LEACHM: A process based model of water and solute movement, transformations, plant uptake and chemical reactions in the unsaturated zone. Chemical equilibrium and reaction models. Proceedings San Antonio, Texas, USA, 23-24 October, pp. 409-422.

https://eurekamag.com/research/002/562/002562948.php (last accessed 22 August 2018).

Jones, J.W., Hoogenboom, G., Porter, C.H., Boote, K.J., Batchelor, W.D., Hunt, L.A., Wilkens, P.W., Singh, U., Gijsman, A.J., Ritchie, J.T., 2003. The DSSAT cropping system model. Eur. J. Agron. 18(3-4), 235-265. DOI: 10.1016/S1161-0301(02)00107-7.

Kahlown, M.A., Azam, M., 2003. Effect of saline drainage effluent on soil health and crop yield. Agric. Water Manage. 62(2), 127-138. DOI: 10.1016/S0378-3774(03)00096-9.

Kumar, P., Sarangi, A., Singh, D.K., Parihar, S.S., Sahoo, R.N., 2015. Simulation of salt dynamics in the root zone and yield of wheat crop under irrigated saline regimes using SWAP model. Agric. Water Manage. 148, 72-83. DOI: 10.1016/j.agwat.2014.09.014.

Li, J., Mao, X., Li, M., 2017. Modeling hydrological processes in oasis of Heihe River Basin by landscape unit-based conceptual models integrated with FEFLOW and GIS. Agric. Water Manage., 179: 338-351. DOI: 10.1016/j.agwat.2016.09.007.

Lima-Vivancos, V., Voller, V.R., 2004. Two numerical methods for modeling variably saturated flow in layered media. Vadose Zone J. 3(3), 1031-1037. DOI: 10.2136/vzj2004.1031.

Ma, H., Yang, D., Lei, H., Cai, J., Kusuda, T., 2011. Application and improvement of Hydrus-1D model for analyzing water cycle in an agricultural field. Trans. CSAE. 27(3), 6-12. DOI: 10.3969/j.issn.1002-6819.2011.03.002.

Ma, L., Hoogenboom, G., Ahuja, L.R., Ascough, J.C., Saseendran, S.A., 2006. Evaluation of the RZWQM-CERES-Maize hybrid model for maize production. Agric. Syst. 87(3), 274-295. DOI: 10.1016/j.agsy.2005.02.001.

McCown, R.L., Hammer, G.L., Hargreaves, J.N.G., Holzworth, D.P., Freebairn, D.M., 1996. APSIM: A novel software system for model development, model testing and simulation in agricultural systems research. Agric. Syst. 50(3), 255-271. DOI: 10.1016/0308-521X(94)00055-V.

Millington, R.J., Quirk, J.P., 1961. Permeability of porous solids. Trans. Faraday Soc. 57, 1200-1207. DOI: 10.1039/TF9615701200

Molden, D., 1997. Accounting for water use and productivity. International Irrigation Management Institute, Colombo, Sri Lanka. DOI: 10.1080/07900629948934.

Monsi, M., Saeki, T., 1953. Uber den Lictfaktor in den Pflanzengesellschaften und sein Bedeutung fur die Stoffproduktion. Jpn. J. Bot. 14, 22-52.

Mualem, Y., 1976. A new model for predicting the hydraulic conductivity of unsaturated porous media. Water Resour. Res. 12(3), 513-522. DOI: 10.1029/WR012i003p00513.

Romano, N., Brunone, B., Santini, A., 1998. Numerical analysis of one-dimensional unsaturated flow in layered soils. Adv. Water Resour. 21(4), 315-324. DOI: 10.1016/S0309-1708(96)00059-0

Salamati, N., Delbari, M., Abbasi, F., Dashtgol, A.S., 2016. Simulation of water and nitrate transport in soil using HYDRUS-1D model in furrow irrigation of sugarcane. J. Water Soil Sci. 19(74), 179-192. DOI: 10.18869/acadpub.jstnar.19.74.15.

Schnabel, R. R., Richie, E. B., 1984. Calculation of internodal conductances for unsaturated flow simulations: A comparison. Soil Sci. Soc. Am. J. 48(5), 1006-1010. DOI: 10.2136/sssaj1984.03615995004800050010x

Shang, S., Mao, X., Lei, Z., Yang, S., 2009. Models and application of soil water dynamics. Beijing: Science Press, China, 185 pp.

Simunek, J., Sejna, M., van Genuchten, M.Th., 1999. The HYDRUS-2D software package for simulating the one-dimensional movement of water, heat, and multiple solutes in variably-saturated media version 2.0. U.S. Salinity Laboratory Agricultural Research Service, U.S. Department of Agriculture, Riverside, California. http://pc-progress.com/Downloads/Pgm_Hydrus2D/HYDRUS2D.PDF (last accessed 22 August 2018).

Simunek, J., van Genuchten, M.Th., Sejna, M., 2005. The HYDRUS-1D software package for simulating the one-dimensional movement of water, heat, and multiple solutes in variably-saturated media version 4.0. Dep. of Environmental Sciences, Univ. of California Riverside, California. https://www.ars.usda.gov/ARSUserFiles/20360500/pdf_pubs/P2119.pdf (last accessed 22 August 2018).

Singh, R., Kroes, J.G., van Dam, J.C., Feddes, R.A., 2006. Distributed ecohydrological modelling to evaluate the performance of irrigation system in Sirsa district, India: I. Current water management and its productivity. J. Hydrol. 329(3-4), 692-713. DOI: 10.1016/j.jhydrol.2006.03.037.

Sophocleous, M., Townsend, M.A., Vocasek, F., Ma, L, Kc, A., 2009. Soil nitrogen balance under wastewater management: Field measurements and simulation results. J. Environ. Qual. 38(3): 1286-1301. DOI: 10.2134/jeq2008.0318.

Srivastava, R., Guzman-Guzman, A., 1995. Analysis of hydraulic conductivity averaging schemes for one-dimensional, steady-state unsaturated flow. Ground Water. 33(6), 946-952. DOI: 10.1111/j.1745-6584.1995.tb00040.x.

Szymkiewicz, A., Helmig, R., 2011. Comparison of conductivity averaging methods for one-dimensional unsaturated flow in layered soils. Adv. Water Resour. 34(8), 1012-1025. DOI: 10.1016/j.advwatres.2011.05.011.

Tuong, T.P., Bhuiyan, S.I., 1999. Increasing water-use efficiency in rice production: Farm-level perspectives. Agric. Water Manage. 40(1), 117-122. DOI: 10.1016/S0378-3774(98)00091-2.

Uchijima, Z., Udagawa, T., Horie, T., Kobayashi, K., 1968. The penetration of direct solar radiation into corn canopy and the intensity of direct radiation on the foliage surface. J. Agric. Meteorol. 24(3), 141-151. https://www.jstage.jst.go.jp/article/agrmet1943/24/3/24_3_141/_pdf (last accessed 22 August 2018).

van Dam, J.C., Huygen, J., Wesseling, J.G., Feddes, R.A., Kabat, P., van Walsum, P.E.V., Groenendijk, P., van Diepen, C.A., 1997. Theory of SWAP version 2.0. DLO Winand Staring Centre, Wageningen, Netherlands. http://www.swap.alterra.nl/DownloadHistory/swap207d/Swap207d%20theory%20(TechDoc%2045).pdf (last accessed 22 August 2018).

van Genuchten, M.Th., 1980. A closed-form equation for predicting the hydraulic conductivity of unsaturated soils. Soil Sci. Soc. Am. J. 44(5), 892-898. DOI: 10.2136/sssaj1980.03615995004400050002x

van Genuchten, M.Th., 1987. A numerical model for water and solute movement in and below the root zone. Research Report No. 121. United States Department of Agriculture Agricultural Research Service US Salinity Laboratory, Riverside, California, USA.

Wang, C., Mao, X., Hatano, R., 2014. Modeling ponded infiltration in distinctly layered soil fine textured soil with coarse interlayer. Soil Sci. Soc. Am. J. 78(3), 745-753. DOI: 10.2136/sssaj2013.12.0535.

Wesseling, J. G., Elbers, J. A., Kabat, P., van den Broek, B. J., (1991). SWATRE: Instructions for input. Report. Wageningen, Netherlands: Winand Staring Cent.

Williams, J.R., Jones, C.A., Kiniry, J.R., Spanel, D.A., 1989. The EPIC crop growth

model. T. ASABE. 32(2), 497-511. DOI: 10.13031/2013.31032.

Xu, X., Huang, G., Sun, C., Pereira, L.S., Ramos, T.B., Huang, Q., Hao, Y., 2013. Assessing the effects of water table depth on water use, soil salinity and wheat yield: Searching for a target depth for irrigated areas in the upper Yellow River basin. Agric. Water Manage. 125(7), 46-60. DOI: 10.1016/j.agwat.2013.04.004.

Xu, X., Sun, C., Huang, G., Mohanty, B.P., 2016. Global sensitivity analysis and calibration of parameters for a physically-based agro-hydrological model. Environ. Modell. Softw. 83, 88-102. DOI: 10.1016/j.envsoft.2016.05.013.

Zhou, J., Cheng, G., Li, X., Hu, B.X., Wang, G., 2012. Numerical modeling of wheat irrigation using coupled HYDRUS and WOFOST models. Soil Sci. Soc. Am. J. 76(2), 648-662. DOI: 10.2136/sssaj2010.0467.